GEUS Report on climate and bedrock permafrost degradation modelling

Contents

Summary

The degradation of bedrock permafrost can alter the stability of steep rock slopes along Greenland's fjords. Starting in 2019, in-situ measurements and climate modelling have been used to produce a first assessment of bedrock permafrost on steep slopes in the region between Disko Island and Svartenhuk Halvø in central West Greenland.

Mean annual air temperature (MAAT) from a 5.5x5.5 km resolution regional climate model provided by DMI was downscaled to a 100x100 m resolution suitable for studying steep slope in complex topography. The strong effect of shadows and illumination angle on incoming solar radiation at the ground surface was parameterized by raytracing and applying a scaling coefficient calibrated to fit the in-situ temperature measurements. Finally, the temperature regime in the bedrock was estimated based on a simple conceptual model, well established in the literature, that relates air temperature to ground surface and subsurface temperatures.

We find that the climate in the last three decades is consistent with most of the landscape in the region being underlain by stable permafrost including at low elevation, except for some south-facing slopes of the fjords on the easternmost part of the region (Fig. 1). As climate warms, projections based on RCP 4.5 (intermediate greenhouse gas concentration trajectory) predict widespread permafrost degradation affecting a large fraction of south facing slopes along the fjords and approaching the margin of the Greenland Ice Sheet.

Under the higher greenhouse gas concentration trajectory represented by RCP 8.5, permafrost degradation will affect most slopes along the fjords, including north facing ones.

The model currently implemented does not attempt to explicitly predict temperature deep into the rock mass, as such a large region would require too much computing power for the scope of the current project. Qualitatively, the timing of permafrost disappearance will increasingly lag surface conditions at increasing depths. Consequently, positive temperature at the top of the permafrost (TTOP) must be understood as indicating ongoing deep permafrost warming and ultimately disappearance over time.

Experimental and theoretical evidence from the literature suggests that the safety factor of a frozen rock slope gradually decreases as temperature increases, with the lowest shear strength at a temperature close to but below the thawing point. At the level of detail of this initial regional assessment, we summarize our modelling results by mapping the estimated mean annual temperature at the top of permafrost (TTOP) into three temperature ranges in Fig. 1:

- solid blue for TTOP below -2°C: slopes gradually get weaker as they warm and this may cause failures, but defining when and where requires a future study that includes the details of local geology, geomechanics and climate
- blue-red shades for TTOP between -2°C and 0°C: slopes in the range of maximum temperature-related loss of shear strength. If a slope is to fail due to shear strength loss from permafrost degradation, it will fail no later than when it reaches within this range, with increasing time lag for increasing depth of the failure surface
- solid red for TTOP above 0°C: slopes that are permafrost-free at increasing depths with time. Previously stable slopes can however still become unstable due to the increased permeability of the unfrozen rock mass.

The main conceptual limitation of the present model formulation is the lack of vertical dimension below the surface, which requires transient modelling of heat propagation and is very computationally expensive over such a large area.

The main limitations of the present results are due to the short timeseries, the non-overlap in time between observations and model, which complicates the calibration of the parameterizations used in the TTOP model, and the well-known difficulty to accurately predict snow depth and the magnitude of its warming effect on mean annual ground surface temperature (MAGST). Acknowledging this limitation, the effect of snow is calculated in a very simplistic way based only on the available automatic weather station (AWS) measurements of MAAT and MAGST. In situ measurements also suggest that the albedo of the outcropping lithologies has a detectable effect on ground heating by solar radiation that is not included in the current implementation of the model.

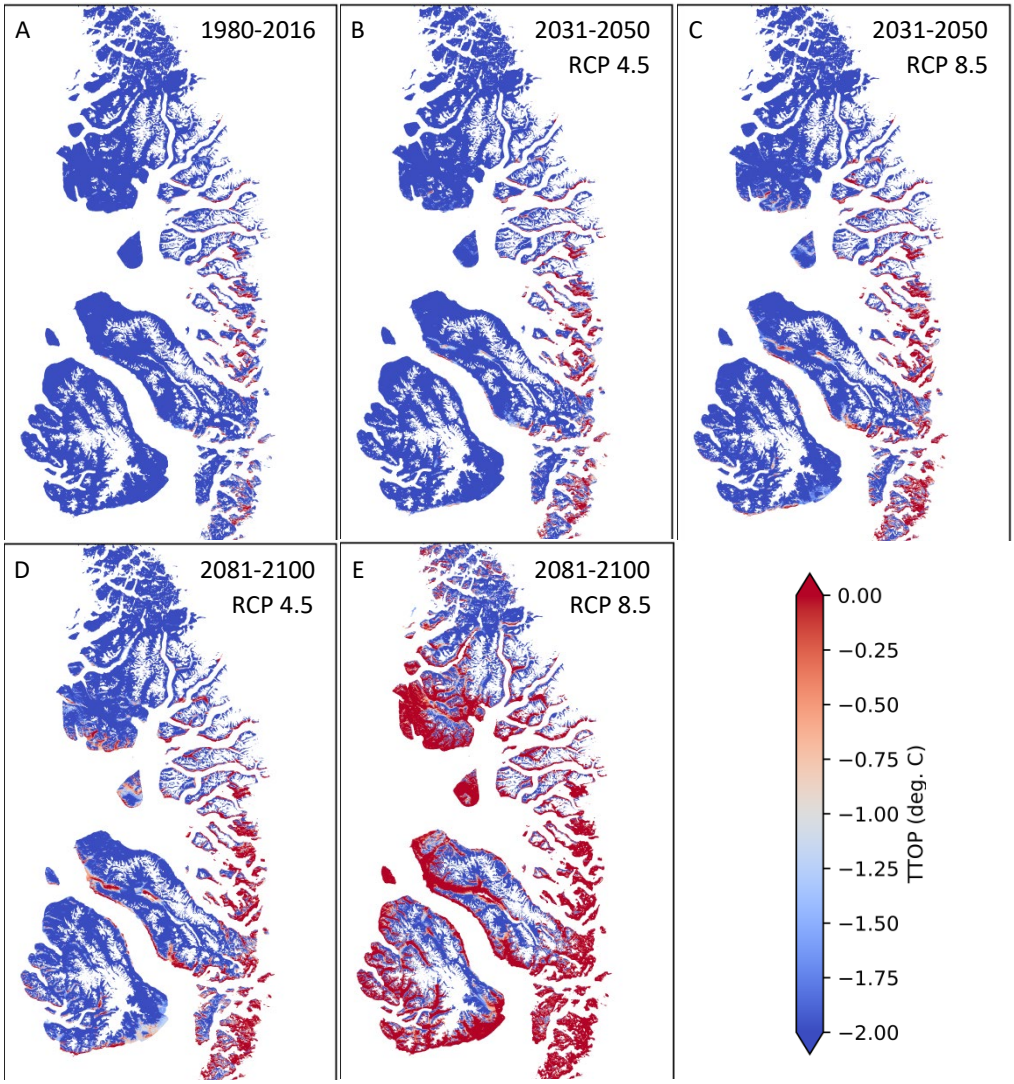

Figure 1: A) Modelled mean annual temperature at the top of permafrost from years 1980–2016 ERA Interim reanalysis climate, B) years 2031–2050 projection based on the RCP 4.5 representative concentration pathway (intermediate greenhouse gas concentration trajectory). C) years 2031–2050 projection based on the RCP 8.5 representative concentration pathway (high greenhouse gas concentration trajectory). D) years 2081–2100 projection based on the RCP 4.5 representative concentration pathway (intermediate greenhouse gas concentration trajectory). E) years 2081–2100 projection based on the RCP 8.5 representative concentration pathway (high greenhouse gas concentration trajectory). Note that the model is formulated specifically for bedrock slopes and, everything else equal, permafrost temperatures can be expected to be lower at sites with deep soil and vegetation cover.

Introduction

The ongoing and projected climate warming is gradually exposing Greenland's landscape to physical conditions that it has not experienced since the Holocene climatic optimum c. 6000 years ago, with temperatures projected to exceed it in the near future. Permafrost degradation in rock slopes can modify the mechanical properties and hydraulic regime of the rock mass and prepare or trigger all magnitudes of slope failures (Krautblatter et al., 2013; Draebing et al., 2014). This process has been inferred to already occur in central West Greenland (Svennevig et al., 2022). Experimental and theoretical evidence from the literature show that the shear strength of ice-filled fractures and joints, and consequently the safety factor of a slope, gradually decrease as temperature increases. While stress and strain regime influence the relationship between temperature and shear strength, this gradual weakening is well documented already from -10°C, reaching a minimum at some temperature between the ice pressure melting point and c. -1°C below it (Davies et al., 2001, Mamot et al., 2018). The exact melting point of ice in bedrock joints and porosity depends on local physical and chemical factors controlled by local geology and the stress field in the rock mass. Bedrock temperature at increasing depths responds to changes of surface temperature with a time lag proportional to depth and the thermal properties of the rock mass. The influence of local surface and subsurface conditions, and the computational requirements for modelling subsurface heat transfer over a large region of complex topography, make it impractical to model these effects in detail at the landscape scale within the scope of a screening project. Furthermore, applying the available theoretical understanding of these physical processes is complicated by the severe lack of field measurements from steep rock slopes, with almost all permafrost research in the Arctic focusing on lowland tundra and soils. In this investigation we therefore collected new in situ measurements and adopted the simplified approach of estimating ground temperature at the depth of the top of permafrost (TTOP), which in this region can be expected to be in the order of a few meters.

The model currently implemented does not explicitly predict temperature deep into the rock mass. Qualitatively, the timing of permafrost disappearance will increasingly lag surface conditions at increasing depths. Consequently, positive TTOP must be understood as indicating ongoing deep permafrost warming and ultimately disappearance over time. Finally, it must be noted that the input climate data to the model is derived from a regional climate model (RCM) rather than directly from in-situ weather observations. This is necessary for three reasons:

- The region of interest is much larger than the representativeness of in situ measurement at the point of any instrument
- We need consistent and gap-free input climate over longer time intervals than individual measurement series can provide
- We need predicted climate under future climate scenarios.

The RCM provides an internally consistent and seamless climate dataset that spans several decades in the past based on data reanalysis (in our case, 1980–2016) and in the future

using different scenarios of atmospheric warming for 2031–2050 and 2081–2100 both under RCP 4.5 and RCP 8.5 (representative carbon pathways).

To increase our understanding of these processes in steep slopes, in 2019 the GEUS Landslides Project established a network of sensors on both sides of the Vaigat Strait described in further details in the next section. This network consists of surface and subsurface ground temperature measurements in 15 boreholes drilled in bedrock slopes. Additional boreholes, including a 6 m deep one, were drilled and instrumented in 2021 by the Thawing Mountains Project, a collaboration between GEUS and DTU funded by Energistyrelsen through DANCEA (Danish Cooperation for Environment in the Arctic).

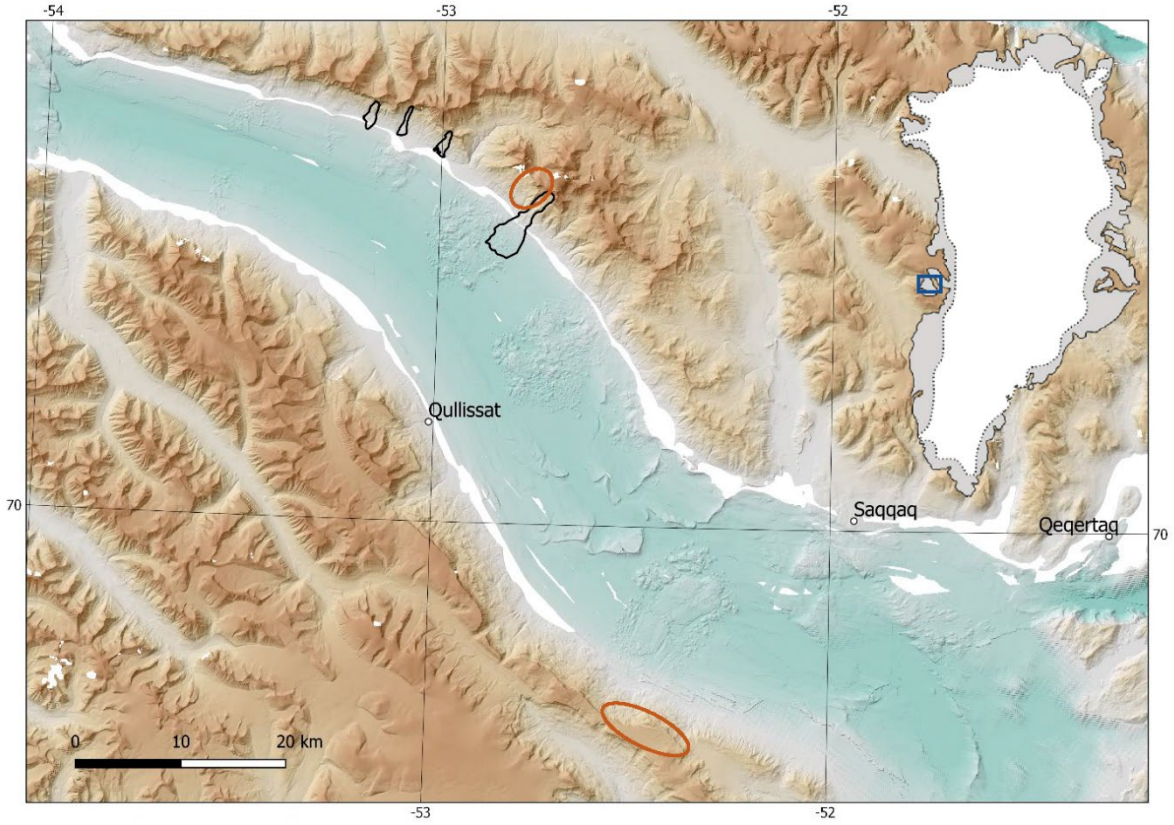

Figure 2: Overview of the location of Vaigat Strait and the two instrumented sites on Disko Island and Nuussuaq Peninsula (orange ellipses). Historical landslides are shown in black outline.

Observations

The in-situ measurements have been produced by installing 15 thermistor strings (TS) and 3 automatic weather stations (AWS) during summer 2019, complemented by time lapse cameras taking daily mages of the site where the sensors were installed so that snow conditions could be qualitatively assessed. Each TS, supplied by GeoPrecision GmbH (Ettlingen, Germany), is drilled into boreholes perpendicular to the surface of the bedrock and composed by a datalogger and a sensor cable with thermistors sensing temperatures at the surface and at depths of 20, 40, 60, 80 and 100 cm at 10 of the 15 TS sites, and also at 150 and 200 cm at the remaining 5 of the TS sites. Data from the dataloggers can be

downloaded over a radio link to simplify fieldwork where access would otherwise require rope technique on vertical rock walls (Fig. 3).

Figure 3: Drilling of bedrock boreholes for measuring the temperature of the rock wall down to 1 m and 2m depth (top left and top right, respectively). Automatic weather stations were installed at different elevations to measure near-surface weather (bottom).

The automatic weather stations use a design adapted from the standard GEUS automatic weather stations used for the monitoring the Greenland Ice Sheet (Fausto et al., 2021), with one station (VAI-1 in Fig. 2, bottom left and middle) extended to include a rain gauge supplied by Geonor AS (Østerås, Norway). The remaining two stations VAI-2 and VAI-3 carry a reduced suite of sensors sufficient for monitoring conditions at sites influenced by nearby slopes (Fig. 3, bottom right). A time series of air temperature (Fig. 4) and a scatter plot showing the relationship between instantaneous air and ground surface temperatures (Fig. 5) provide examples of the data produced by these stations for use in model calibration. It can be seen that winter air temperatures at VAI-1 can reach below -30°C but ground surface, being protected by the insulating effect of the snow cover, never drops below -20ºC.

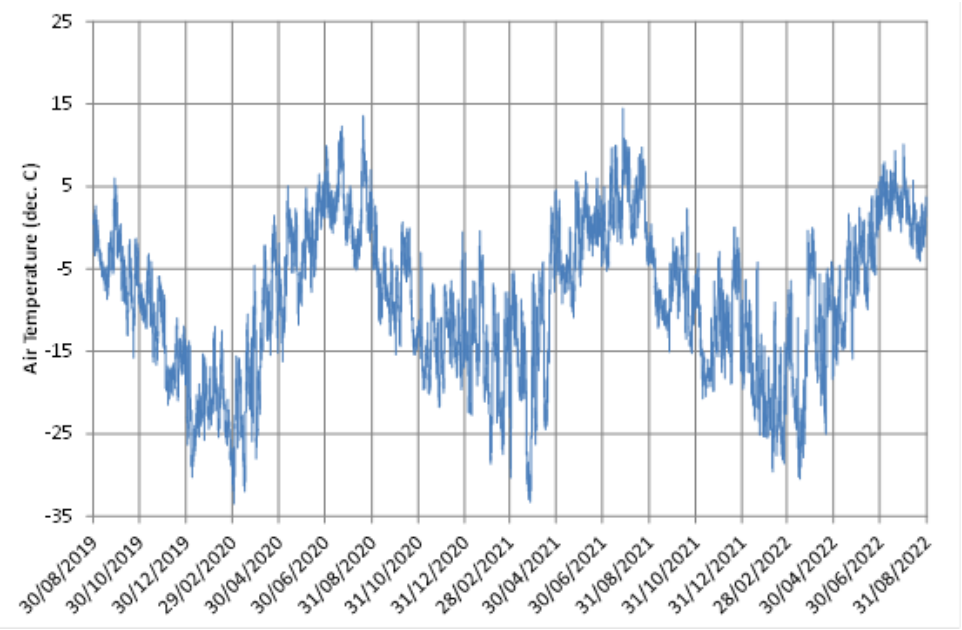

Figure 4: Air temperature recorded at the VAI-1automatic weather station at 1176 m a.s.l. on Disko Island for the period September 2019 – August 2022.

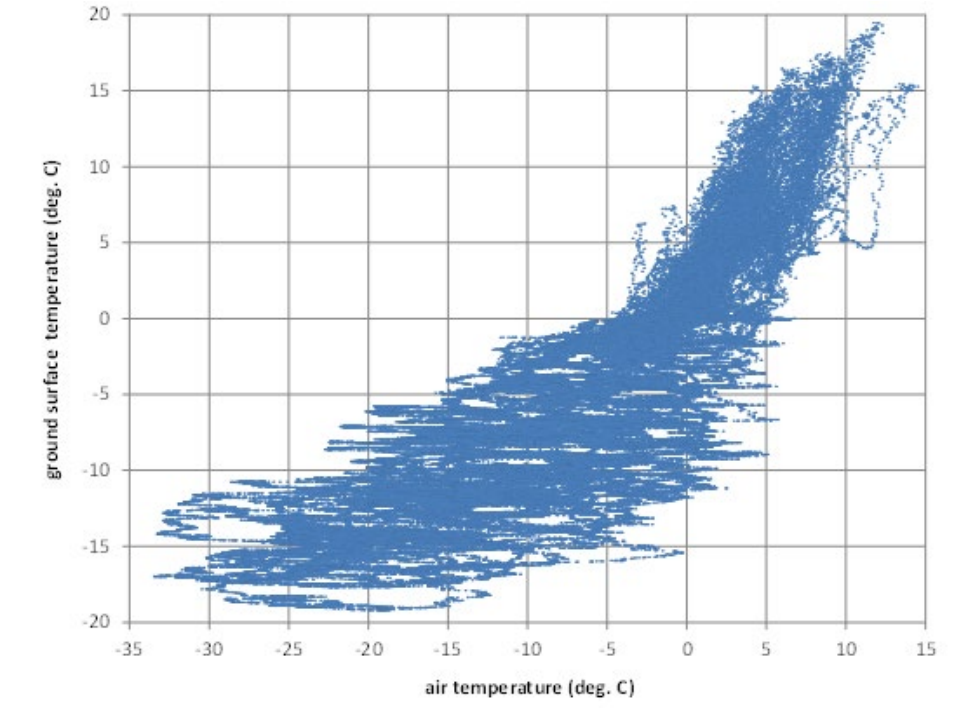

Figure 5: Relation between surface temperature and air temperature recorded at the VAI-1automatic weather station at 1176 m a.s.l. on Disko Island for the period September 2019 – August 2022.

The thermistor strings data show that in this region the thickness of the active layer that thaws every year is in excess of 2 metres, with only the 6 m long A53CE5 borehole reaching into the underlying permafrost. Figures 6–9 show the complete ground temperature records, measured every hour. At the surface, temperature responds rapidly to air

temperature and insolation while the temperature signal becomes increasingly smoothed and delayed as depth increase. The average difference between air and ground temperature (nival offset) over 36 consecutive months is 2.51 °C.

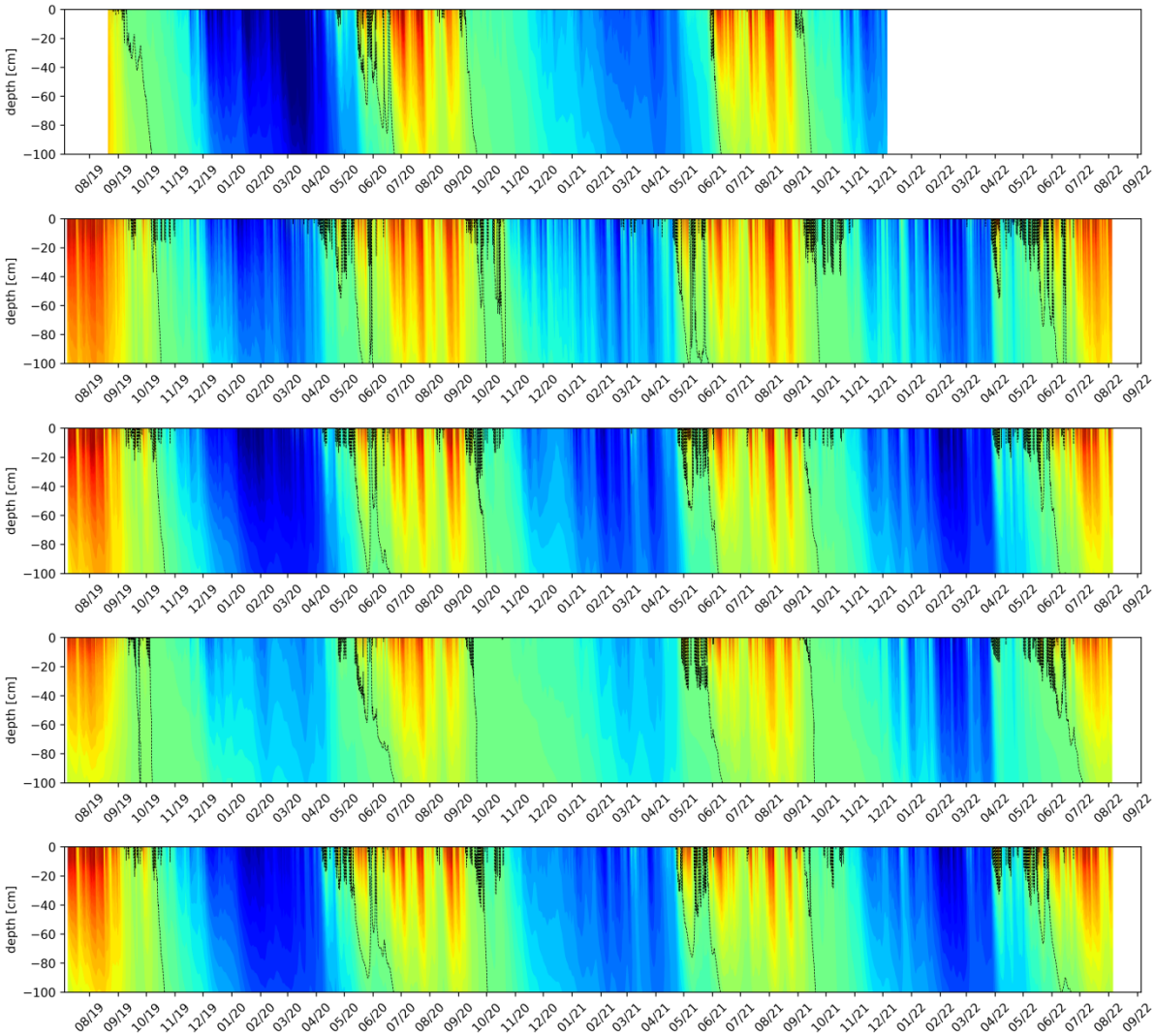

Figure 6: Temperature versus depth of thermistor strings A53ADF, A53AE0, A53AE1, A53AE2, A53AE3 drilled in 1 m long boreholes for the period July 2019 – August 2022. The color scale ranges from -20°C (dark blue) to +20°C (dark red), the black line marks 0°C.

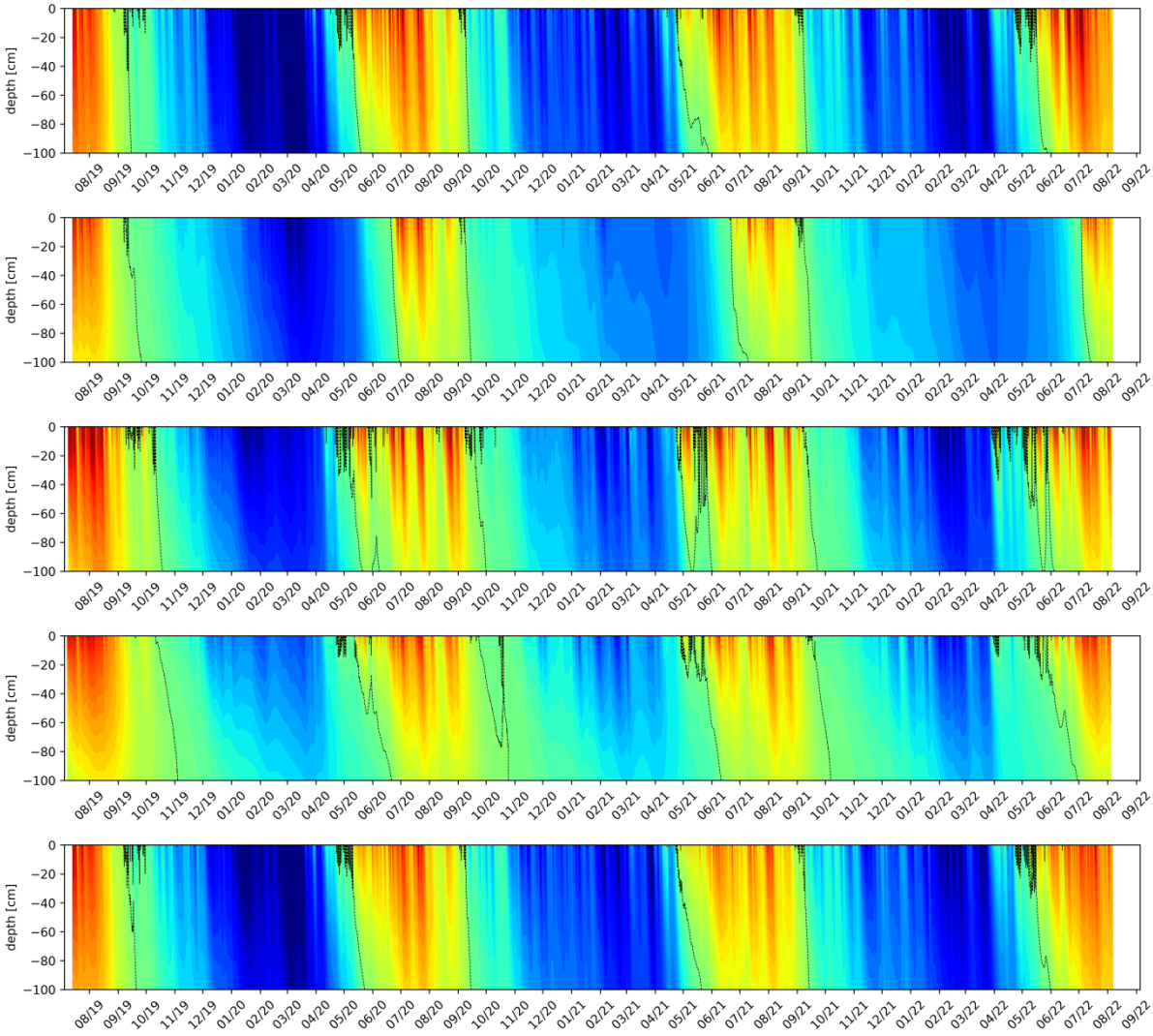

Figure 7: Temperature versus depth of thermistor strings A53AE4, A53AE5, A53AE6, A53AE7, A53AE8, drilled in 1 m long boreholes for the July August 2019 – August 2022. The color scale ranges from -20°C (dark blue), the black line marks 0°C.

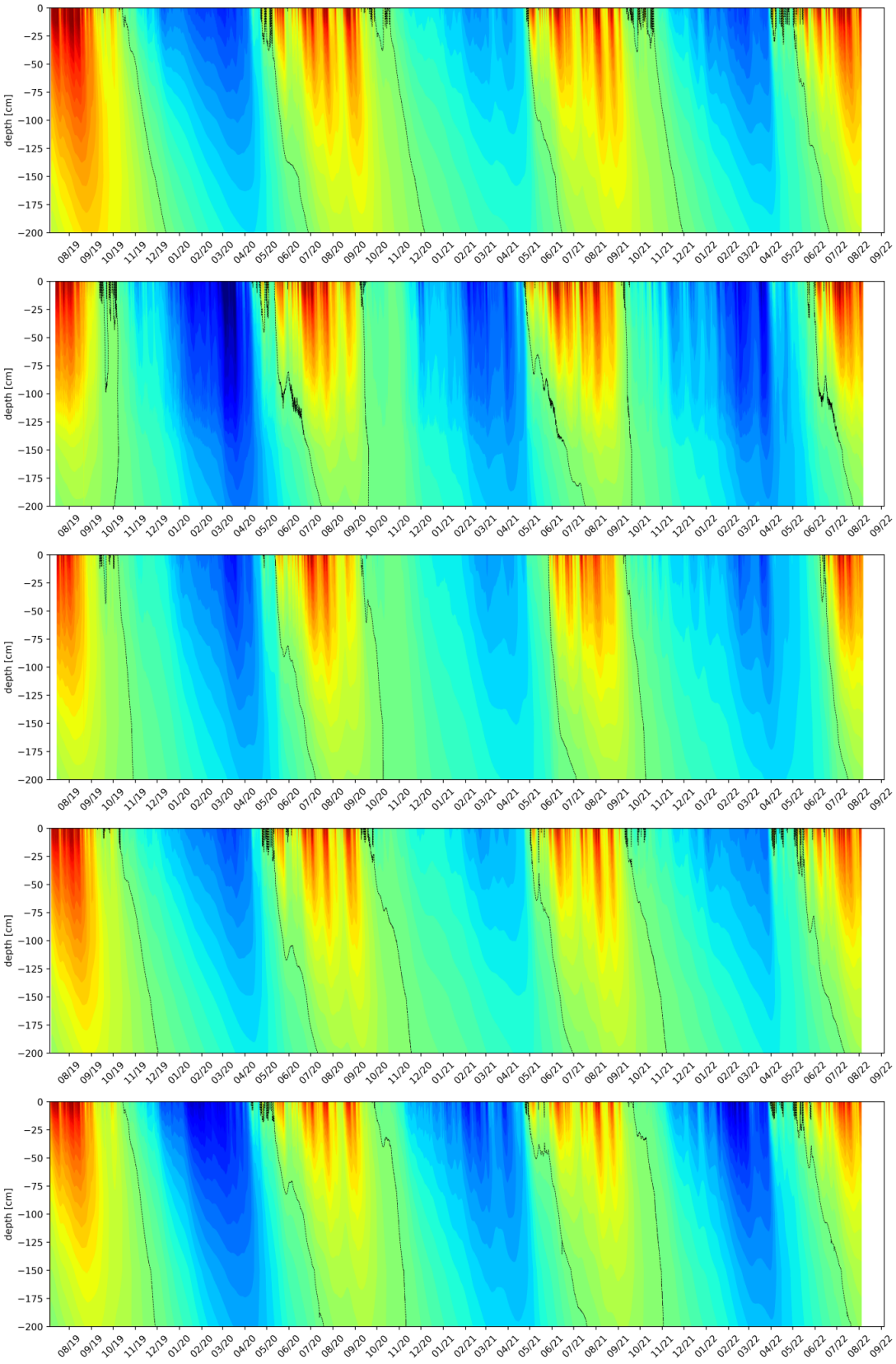

Figure 8: Temperature versus depth of thermistor strings A53AE9, A53AEA, A53AEB, A53AEC, A53AED drilled in 2 m long boreholes for the period July 2019 – August 2022. The color scale ranges from -20°C (dark blue), the black line marks 0°C.

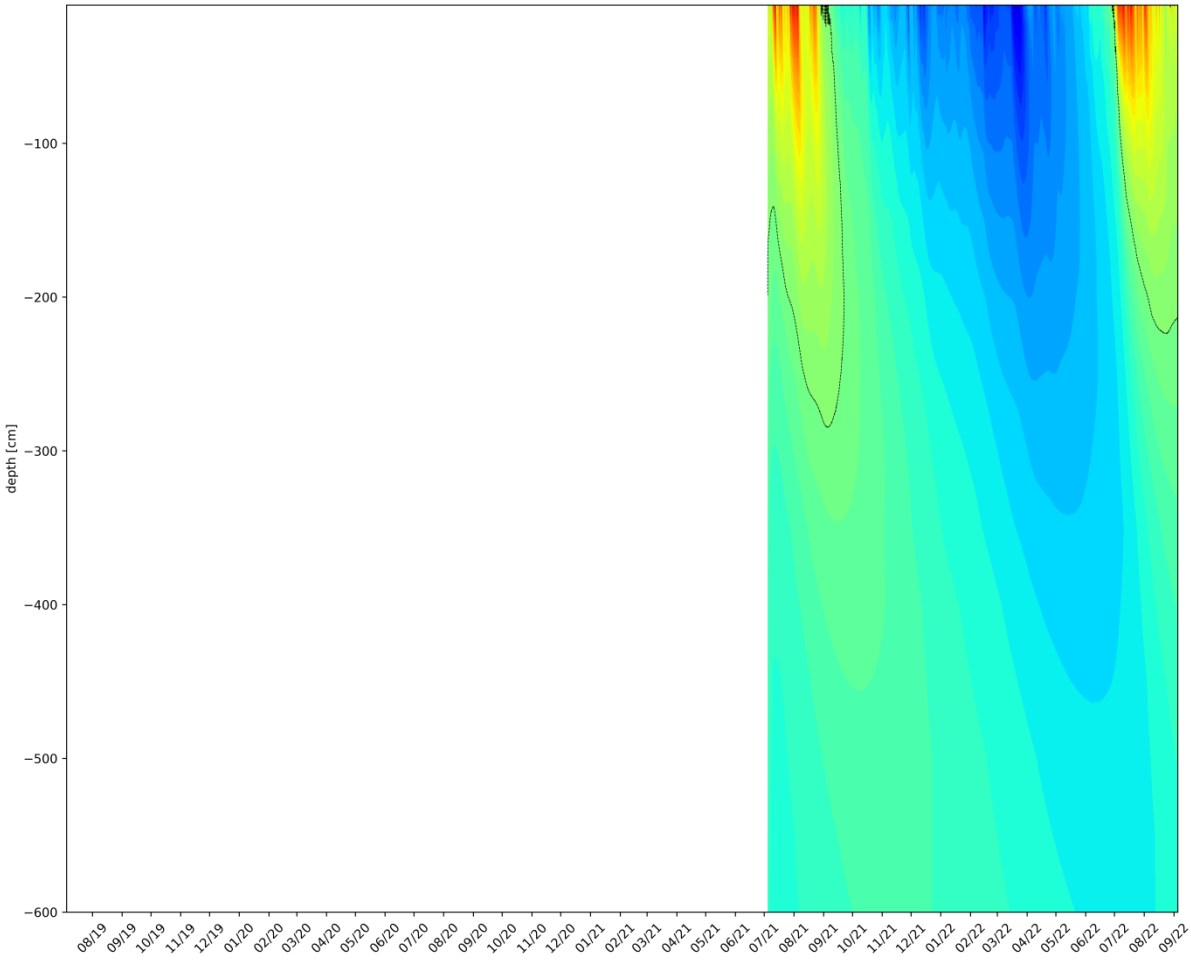

Figure 9: Temperature versus depth for the period July 2021 – September 2022 of thermistor string A53CE5 from a 6 m long borehole drilled in collaboration with the Thawing Mountains research project. The color scale ranges from -20°C (dark blue) to +20°C (dark red), the black line marks 0°C.

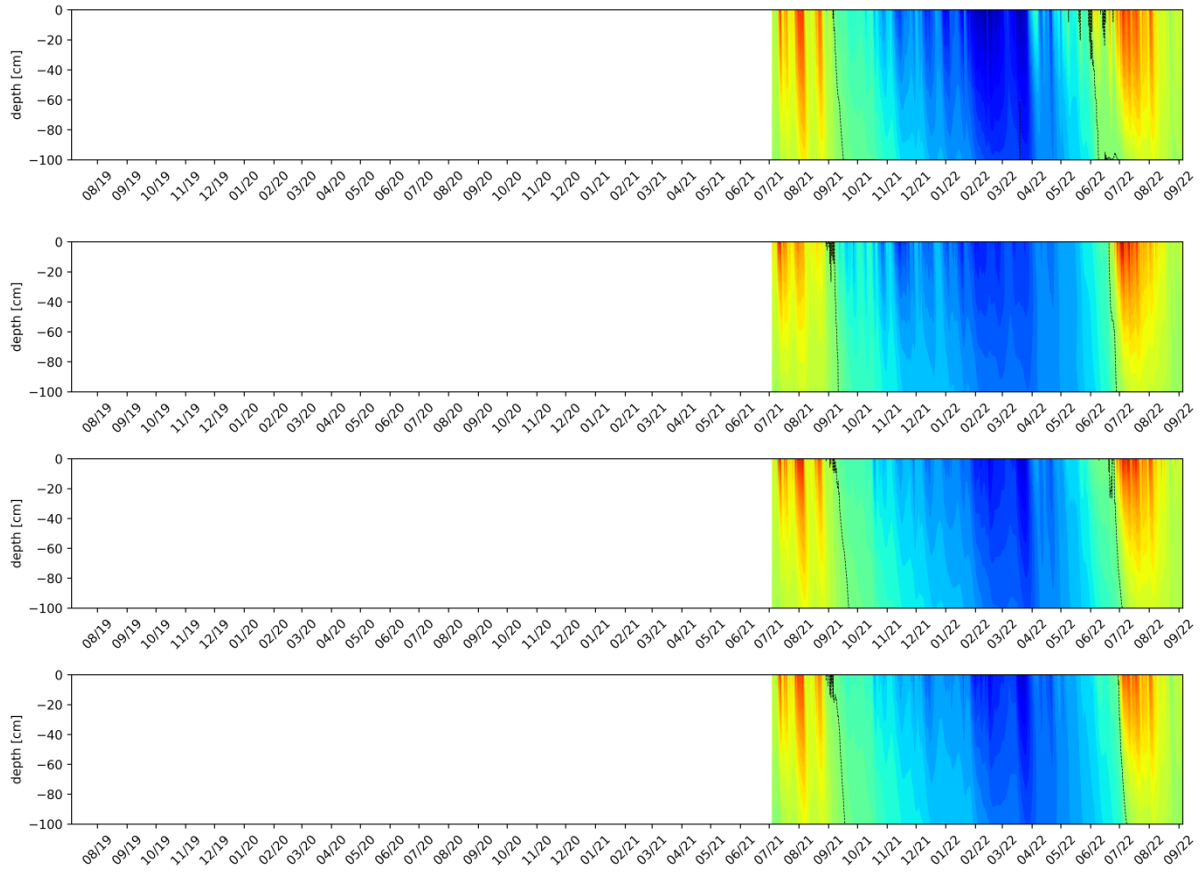

Figure 10: Temperature versus depth for the period July 2021 – September 2022 of thermistor strings A53E3E, A53E3F, A53E41, A53E42 drilled in 1 m long boreholes in collaboration with the Thawing Mountains research project. The color scale ranges from -20°C (dark blue) to +20°C (dark red), the black line marks 0°C.

Across all boreholes and years, the ground temperature difference between 1 m depth and the surface is on average -0.22 ºC (median -1.19, range -1.19 to +0.29) while at 2 m depth the surface is on average -0.25 ºC (median -1.11, range -1.22 to +0.45). The top of the permafrost was found c. 2.5–3 m below the surface at the only 6 m long borehole (A53CE5 shown in Figure 9). These observations confirm that in bedrock the thermal offset due to the higher thermal conductivity of ice compared to water is low, and almost entirely established close to surface.

Figure 11: Time lapse images showing snow encrusting a vertical rock wall (top, A53AE5 thermistor string) and the effect of a small ledge on accumulating more snow (bottom, A53AED thermistor string).

The presence or absence of snow has an insulating effect that slows the cooling of the ground. While it is sometimes assumed in the literature that steep rock walls remain free of snow, the time lapse cameras installed at each thermistor string borehole show that snow can easily encrust the rock wall (Figure 11, top, from the A53AE5 thermistor string). Any small ledge in the slope can also easily accumulate snow (Figure 11, bottom, from the A53AED thermistor string).

Modelling

The model used in this work consists of two main steps:

1) downscaling of air temperature of the regional climate model (RCM) climate grids provided by DMI to a spatial resolution that makes it possible to satisfactorily reproduce the complex and steep topography of the region.
2) estimating ground surface and subsurface temperatures

In the first step, the RCM grids produced by DMI using the HIRHAM5 model are downscaled from 5.5 x 5.5 km to 100 m x 100 m spatial resolution using the same approach as in Citterio

et al. (2017). The local air temperature lapse rate is estimated by least squares linear regression within a 'land' surface type neighborhood of grid cells around each RCM grid cell. The elevation bias is then removed by adding the local lapse rate multiplied by the elevation difference between each 100m resolution grid cell and the 5.5 km it falls within. Due to approximately half of the grid cells along the shoreline being modelled as 'sea' in the RCM, an additional step is carried out to fill these cells using values interpolated from their neighborhood of 'land' surface-type cells, after which the elevation bias from sea level to the actual elevation of the topography is removed as described above. Terrain effects on insolation at the surface due to steep topography and cast shadows are parameterized as a function of potential incoming shortwave radiation (PISWR), calculated at every grid using SAGA GIS by ray tracing from the position of the sun to every 100 m x 100 m grid cell, multiplied by a coefficient calibrated using in-situ observations. The available HIRHAM5-ERAI reanalysis RCM dataset does not overlap in time with our in-situ measurements, and the newer CARRA RCM dataset is not suitable for this application because the only output values made available are averages over all surface types within each grid cell, weighed by their surface fraction. We therefore calibrate the coefficient relating PISWR and surface temperature by means of ordinary least squares multiple regression between measured ground temperature at the thermistor strings as the dependent variable and elevation and PISWR as independent variables (Table 1).

OLS Regression Results

Dep. Variable:	magt_100	R-squared:				0.539
Model:	OLS	Adj. R-squared:				0.517
No. Observations:	45	AIC:				142.7
	coef	std err	t	P>|t|	[0.025	0.975]
const	-1.5162	0.522	-2.903	0.006	-2.570	-0.462
elevation	-0.0019	0.001	-3.604	0.001	-0.003	-0.001
piswr	3.4922	0.511	6.838	0.000	2.462	4.523

OLS Regression Results

Dep. Variable:	magt_100	R-squared:				0.594
Model:	OLS	Adj. R-squared:				0.572
No. Observations:	39	AIC:				120.9
	coef	std err	t	P>|t|	[0.025	0.975]
const	0.0516	0.734	0.070	0.944	-1.437	1.540
elevation	-0.0033	0.001	-4.732	0.000	-0.005	-0.002
piswr	4.7491	0.655	7.256	0.000	3.422	6.077

Table 1: Ordinary least squares multiple regression results including all boreholes (left) and excluding the two boreholes drilled into sandstone (right).

The performance of the multiple regression in terms of R-squared improves when excluding the two thermistor strings A53AE2 and A53AE0 which are drilled in sandstone with higher albedo than at the remaining sites. This is consistent with the expectation that albedo would

play a role in surface warming by solar radiation. Lacking an albedo map covering the region of interest, we neglect this effect.

In the second step we follow the conceptual approach described by Smith and Riseborough (2002) to estimate the temperature at the top of permafrost (TTOP) using surface temperature and offsets representing the effects of the snow cover, vegetation, and the change in thermal conductivity of the ground between frozen and thawed states of the active layer (Fig. 12).

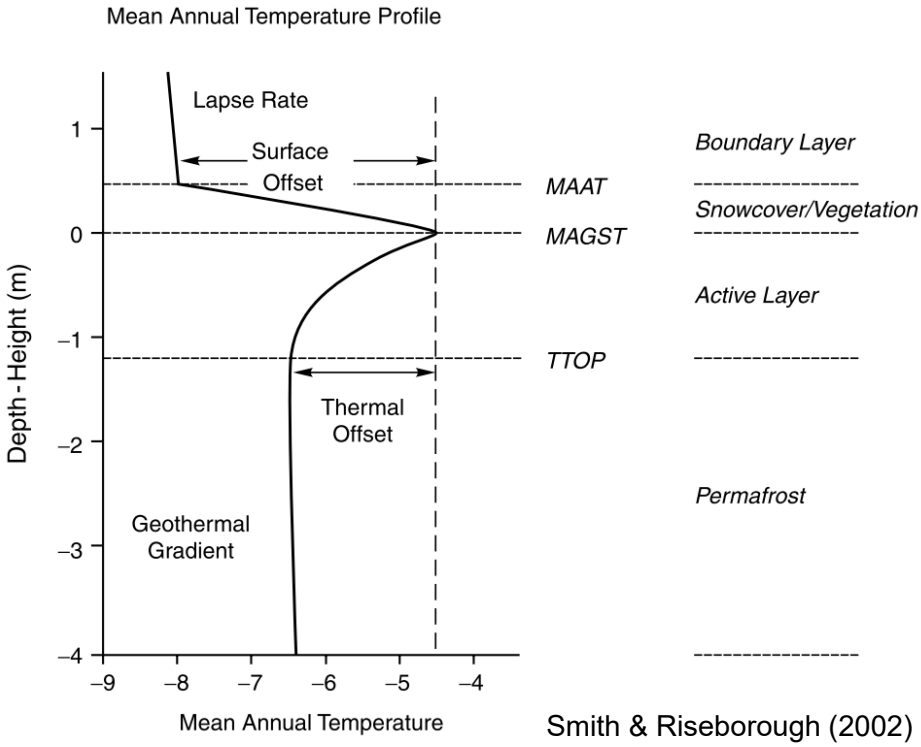

Figure 12: Schematic representation of mean annual temperature profile showing the temperature offsets from the surface to the top of the permafrost in the TTOP model of Smith and Riseborough (2002).

The TTOP approach delivers an approximate mean annual ground temperature at the depth corresponding to the top of the permanently frozen ground under the strong assumption that the ground thermal regime is in thermal equilibrium with the applied surface forcing data (Westermann et al., 2015). This assumption is not strictly verified under ongoing climate change, but the errors are generally expected to be small compared to the other uncertainties, making TTOP adequate for use over larger regions (Westermann et al., 2015; Obu et al., 2019). The implementation of the TTOP model described by Smith and Riseborough (2002) requires scaling factors for snow and vegetation and the thermal conductivity ratio between thawed and frozen ground. Based on these, and air temperature data, the surface and thermal offsets are estimated. In this study we take advantage of our in-situ measurements to directly calculate the magnitude of some of these offsets. Furthermore, our focus on rock slopes allows us to neglect the vegetation effect. Also,

estimating the depth of the snow cover in steep and complex terrain is difficult and uncertain. Therefore, we estimate TTOP by using the observed values described above for nival offset and thermal offset, setting vegetation effects to zero.

As is the general case with TTOP approaches, this is a simple equilibrium model neglecting the history of ground conditions and the time lag from climate forcing at the surface to changing temperatures at depth. The resulting inaccuracies are expected to be more severe close to 0 ºC in a soil rich in moisture (Obu et al., 2019), while in our study we focus on bedrock.

Results

As described in the Modelling section, the first step aims downscaling air temperature to 100 x 100 m spatial resolution, which allows capturing the details of the landscape, and the second step applies the temperature offsets leading from air temperature to temperature at the top of permafrost (TTOP). Figure 13 illustrate the result of the first step, downscaled mean annual air temperature (MAAT) in the left panel, and the end result of the model as TTOP in the right panel. These grids are based on ERA Interim reanalysis climate over the 1980–2016 period.

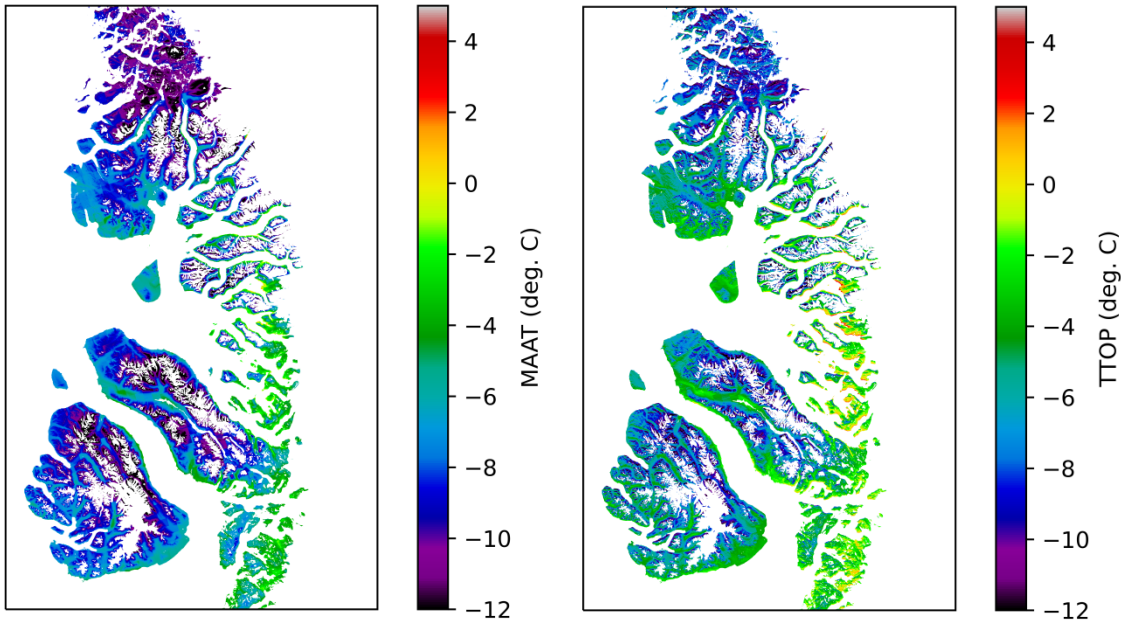

Figure 13: Downscaled mean annual air temperature (MAAT, left panel) and modelled temperature at the top of permafrost (TTOP, right panel) based on a DMI regional climate model forced by climate reanalysis between 1980 and 2016. The MAAT downscaling corrects the elevation bias in the regional climate model. The TTOP model additionally accounts for the effects of snow and the topography control on incoming solar radiation.

In order to predict TTOP during the course of the current century, we use HIRHAM5 grids produced under the RCP 4.5 and RCP 8.5 representative concentration pathway scenarios,

respectively an intermediate and a high emission scenario. We first remove the offset between available HIRHAM5 runs that used different initializations by estimating their difference during the overlapping 1991–2010 period and removing it in the scenario runs. Finally, we obtain the downscaled TTOP grids both shown in Figure 14 for both the 2031–2050 and the 2081–2100 periods. These figures show the same results as Figure 1 but with an extended color scale spanning a larger range of values.

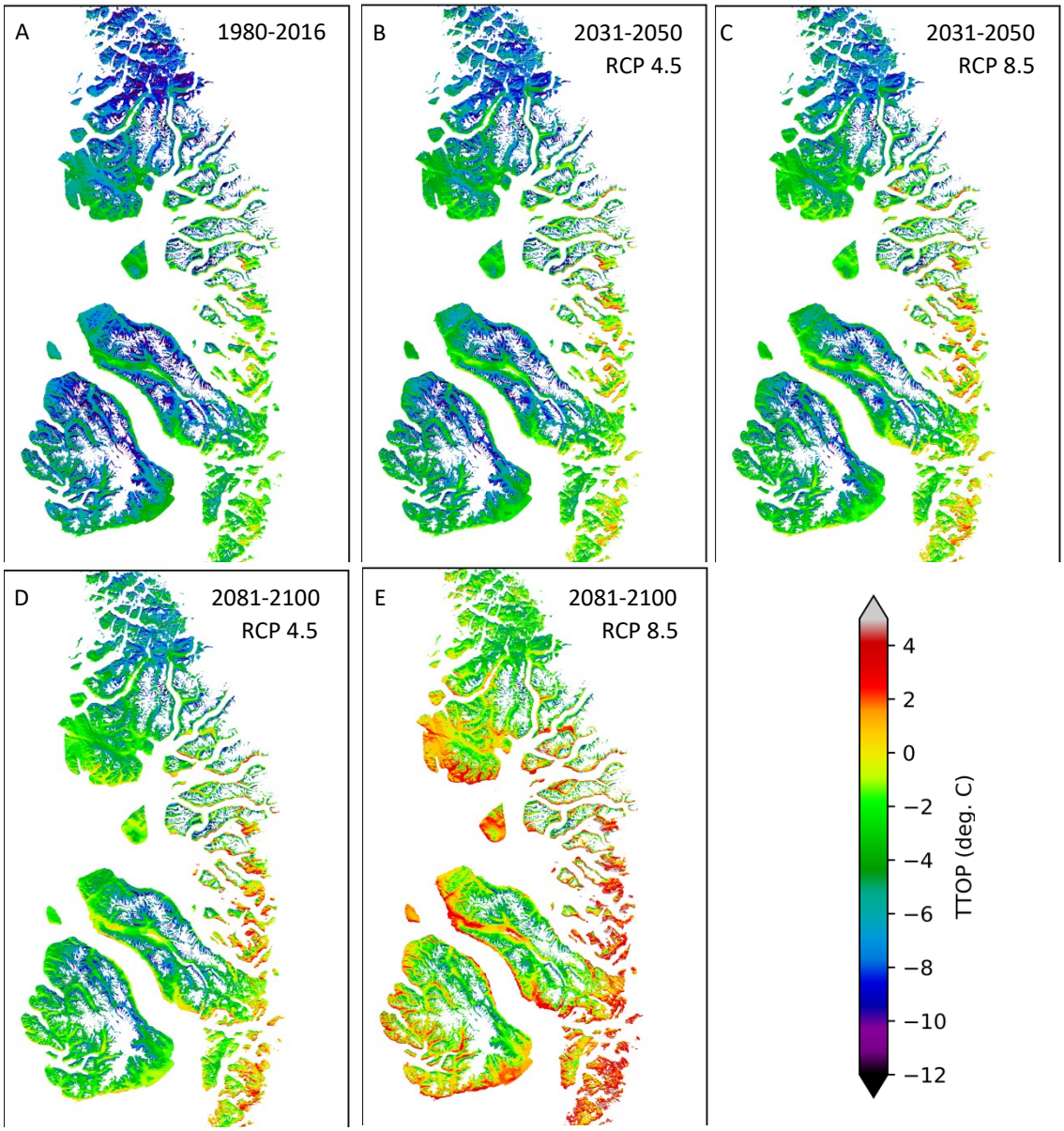

Figure 14: A) Modelled temperature at the top of permafrost from years 1980–2016 ERA Interim reanalysis climate, B) years 2031–2050 projection based on the RCP 4.5 representative concentration pathway (intermediate greenhouse gas concentration trajectory). C) years 2031–2050 projection based on the RCP 8.5 representative concentration pathway (high greenhouse gas concentration trajectory). D) years 2081–2100 projection based on the RCP 4.5 representative concentration pathway (intermediate greenhouse gas concentration trajectory). E) years 2081–2100 projection based on the RCP 8.5 representative concentration pathway (high greenhouse gas concentration trajectory). Note that the model is formulated specifically for bedrock slopes and, everything else equal, permafrost temperatures can be expected to be lower at sites with deep soil and vegetation cover.

Conclusions

Figure 14 shows that the climate in the last three decades is consistent with most of the landscape in the region being underlain by stable permafrost including at low elevation, except for some south-facing slopes of the fjords on the easternmost part of the region. Considering local variability in ground properties, snow depth, insolation and vegetation, this suggests the region encompasses the northern limit of discontinuous permafrost transitioning to continuous permafrost. This is largely consistent with earlier and coarser permafrost zonations such as Westergaard-Nielsen (2018).

As climate warms, projections based on RCP 4.5 (intermediate greenhouse gas concentration trajectory) predict widespread permafrost degradation affecting a large fraction of south facing slopes along the fjords and approaching the margin of the Greenland Ice Sheet. Under the higher greenhouse gas concentration trajectory represented by RCP 8.5 most slopes along the fjords, including north facing ones. Qualitatively, the timing of permafrost disappearance will increasingly lag surface conditions at increasing depths. Consequently, positive TTOP must be understood as indicating ongoing deep permafrost warming and ultimately disappearance over time.

The main limitations of the present results are due to the short timeseries, the non-overlap in time between observations and model which complicates the calibration of the parameterizations used in the TTOP model, and the difficulty to accurately predict snow depth and the magnitude of its warming effect on mean annual ground surface temperature (MAGST). Finally, in situ measurements suggest that the albedo of the outcropping lithologies has a detectable effect on ground heating by solar radiation, but it could not be included in the current implementation of the model.

Future work

The next steps of this research should prioritize implementing a regional climate model dataset overlapping in time with the in-situ measurements, improving the treatment of snow and ground albedo, and ensuring that the time series from this unique Greenland in situ observation network remain operational.

At a later stage, the conceptual formulation of the ground temperature model should move from the TTOP equilibrium model to a transient model capable of explicitly accounting for the past thermal history of the bedrock and for the lag between surface and temperature changes at depth.

References

Citterio, Michele, Mikael K. Sejr, Peter L. Langen, Ruth H. Mottram, Jakob Abermann, Signe Hillerup Larsen, Kirstine Skov, and Magnus Lund. 'Towards Quantifying the Glacial Runoff Signal in the Freshwater Input to Tyrolerfjord–Young Sound, NE Greenland'. Ambio 46, no. 1 (1 February 2017): 146–59. https://doi.org/10.1007/s13280-016-0876-4.

Davies, Michael C. R., Omar Hamza, and Charles Harris. 'The effect of rise in mean annual temperature on the stability of rock slopes containing ice-filled discontinuities'. Permafrost and Periglacial Processes 12, no. 1 (1 March 2001): 137–44. https://doi.org/10.1002/ppp.378.

Fausto, Robert S., Dirk van As, Kenneth D. Mankoff, Baptiste Vandecrux, Michele Citterio, Andreas P. Ahlstrøm, Signe B. Andersen, et al. 'Programme for Monitoring of the Greenland Ice Sheet (PROMICE) Automatic Weather Station Data'. Earth System Science Data 13, no. 8 (6 August 2021): 3819–45. https://doi.org/10.5194/essd-13-3819-2021.

Krautblatter, Michael, Daniel Funk, and Friederike K. Günzel. 'Why Permafrost Rocks Become Unstable: A Rock-Ice-Mechanical Model in Time and Space: A ROCK-ICE-MECHANICAL MODEL FOR PERMAFROST ROCKS'. Earth Surface Processes and Landforms 38, no. 8 (30 June 2013): 876–87. https://doi.org/10.1002/esp.3374.

Mamot, Philipp, Samuel Weber, Tanja Schröder, and Michael Krautblatter. 'A Temperature- and Stress-Controlled Failure Criterion for Ice-Filled Permafrost Rock Joints'. The Cryosphere 12, no. 10 (17 October 2018): 3333–53. https://doi.org/10.5194/tc-12-3333-2018.

Obu, Jaroslav, Sebastian Westermann, Annett Bartsch, Nikolai Berdnikov, Hanne H. Christiansen, Avirmed Dashtseren, Reynald Delaloye, et al. 'Northern Hemisphere Permafrost Map Based on TTOP Modelling for 2000–2016 at 1 Km2 Scale'. Earth-Science Reviews 193 (June 2019): 299–316. https://doi.org/10.1016/j.earscirev.2019.04.023.

Svennevig, Kristian, Reginald L. Hermanns, Marie Keiding, Daniel Binder, Michele Citterio, Trine Dahl-Jensen, Stefan Mertl, Erik Vest Sørensen, and Peter H. Voss. 'A Large Frozen Debris Avalanche Entraining Warming Permafrost Ground—the June 2021 Assapaat Landslide, West Greenland'. Landslides, 23 July 2022. https://doi.org/10.1007/s10346-022-01922-7.

Westergaard-Nielsen, Andreas, Mojtaba Karami, Birger Ulf Hansen, Sebastian Westermann, and Bo Elberling. 'Contrasting Temperature Trends across the Ice-Free Part of Greenland'. Scientific Reports 8, no. 1 (25 January 2018): 1586. https://doi.org/10.1038/s41598-018-19992-w.

Westermann, S., T. I. Østby, K. Gisnås, T. V. Schuler, and B. Etzelmüller. 'A Ground Temperature Map of the North Atlantic Permafrost Region Based on Remote Sensing and Reanalysis Data'. The Cryosphere 9, no. 3 (23 June 2015): 1303–19. https://doi.org/10.5194/tc-9-1303-2015.